ChemComm

Accepted Manuscript

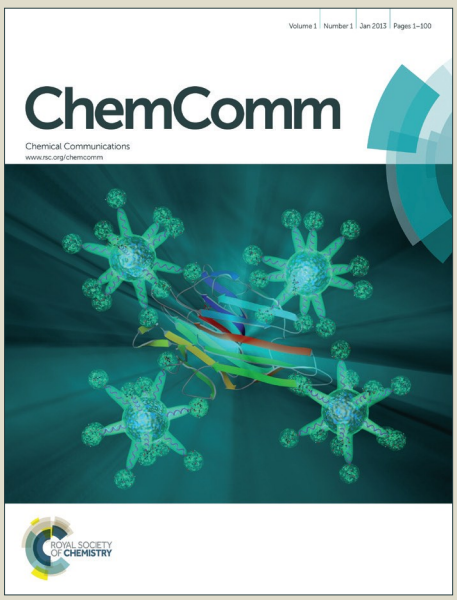

ROYAL SOCIETY OF CHEMISTRY

www.rsc.org/chemcomm

Journal Name

RSCPublishing

COMMUNICATION

Preparation of catalytic films of the Au nanoparticles-carbon composite tubular arrays

Cite this: DOI: 10.1039/x0xx00000x

Wei Gong,[a] Lei Su*[,a] and Xueji Zhang*[,a]

Received ooth January 2012,
Accepted ooth January 2012

DOI: 10.1039/x0xx00000x

www.rsc.org/

Catalytic films comprising the arrayed mesoporous and big-inner-diameter carbon nanotubes embedded with high density Au nanoparticles were prepared through a template-directed carbonization route.

Polydopamine (PDA) films has recently been used in template-directed carbonization to produce hollow carbon spheres, triggering a great deal of interest in synthesizing nanocarbons with versatile morphologies.[1] As carbon source, PDA is environmental-friendly, e.g., its polymerization does not require formaldehyde as cross-linker. Moreover, the PDA films and the resultant carbon shells can exhibit micro-/mesoporous properties, allowing for facile diffusion of reagents in and out of the shells,[2] which is very beneficial for applications, e.g. in catalysis. As a result, metal nanoparticles (NPs) have further been incorporated into these hollow nanocarbons, for instance, to form core-shell or yolk-shell structured composite nanoparticles.[3] These composite nanoparticles can efficiently protect the embedded metal NPs from the notorious aggregation and leakage, providing an outstanding stability to the active catalyst NPs. However, they are usually recycled by tedious and time-consuming centrifugation/redispersion cycles, thus hampering the recovery and reusability of catalysts in liquid solutions.

Compared with the solution-based catalysts, thin films embedded with metal NPs possess more favorable properties from a practical viewpoint.[4] For instance, switching the reaction off or on by the catalytic thin films is technically easier to realize. Moreover, it is easier to separate the catalyst thin films from the reaction solutions, offering the feasibility and ease of multiple reuse. Therefore, there is keen interest in developing thin films, especially possessing three-dimensional (3D) architecture, embedded with metal NPs for catalytic applications. So far, strategies have been developed to construct 3D architecture for preparation of catalytic thin films.[4, 5] Particularly, the arrayed nanotubes modified films have been used for metal NPs deposition for catalytic applications.[6] However, the catalyst NPs were attached onto the outer surface of the sidewalls of the nanotubes,[7] which often suffer from the NP leakage from the films, resulting in the low recyclability of the catalytic films. Alternatively, the insertion of NPs inside the nanotubes seems effective for solving the problem of the NP leakage,[8] but technically challenging in selectively inserting the NPs inside the tubes attached on a substrate.[9] Moreover, the conventional nanotubes, e.g., the carbon nanotubes (CNTs) prepared with chemical vapor deposition and arc discharge methods, have compact sidewalls. As a result, the reagents have to diffuse into the narrow tubes to have access to the embedded catalytic active sites, greatly limiting the catalytic performance of the NP-embedded nanotubes films.

In the present study, we report a template-directed PDA carbonization method for large-area preparation of the AuNP-embedded, mesoporous and big-inner-diameter carbon nanotube array films. This method is simple and facile, and takes full advantage of the merit of the template-directed carbonization route as well as the properties of the carbonized PDA. In this method, ZnO nanorods (NRs) array films were used both as the substrate for attaching AuNP and as the template for carbonization synthesis of the arrayed mesoporous, big-inner-diameter carbon nanotubes (pBIDI-CNTs). As schematically illustrated in Scheme 1, the high density AuNPs were deposited on the arrayed ZnO NRs substrate via a simple sputtering approach (step a). Then, the PDA thin films were used to coat these AuNPs-decorated ZnO NRs (step b), followed by template-directed carbonization of PDA (step c) and acid-induced etching of ZnO (step d). As a result, these NPs were collectively and selectively incorporated inside the formed pBIDI-CNTs, forming the arrayed tubular nanoreactors films.

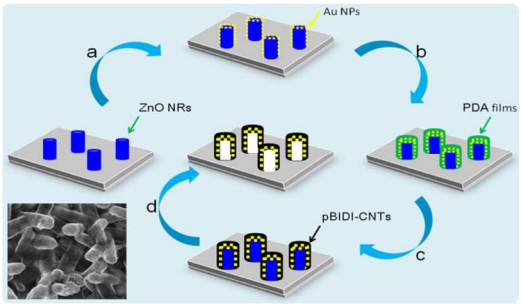

Scheme 1. Schematic illustration of selective attachment of AuNPs onto the inner surfaces of the arrayed pBIDI-CNTs: (a) sputtering deposition of AuNPs on the arrayed ZnO NRs; (b) PDA coating; (c) carbonization of PDA at 500 ^{o}C in N_2 for 3 hs; (d) removal of ZnO NRs in 0.24 M HCl solution for 10 min. Inset shows the real pattern of the obtained AuNPs-embedded pBIDI-CNTs arrays.

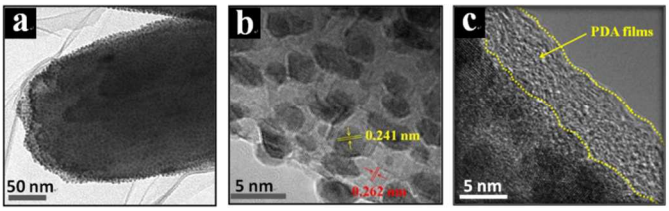

Fig. 1 (a and b) Different magnification TEM images of the AuNPs deposited on the ZnO NRs; (c) side-view TEM image of the Au NPs-decorated ZnO NRs coated with PDA films.

Sputter deposition method is simple and rapid, and the coverage of the attached NPs can be controlled just by using different sputtering time at a fixed current. After 10 s sputtering at 6 mA, a single layer of uniformly distributed AuNPs with about 3.6 nm in average diameter and 0.92 nm in standard deviation (σ) of the NP size distribution, measured over 200 particles, was seen on the surfaces of the ZnO NRs, as shown in Fig. 1 (a-b) and Fig. S1. The particle number density reached a level of ~ 5.9×10^{16} NPs · m^{-2}. As revealed by Fig. 1b, the measured fringe spacing of the NPs was 0.241 nm, which corresponds closely with the spacing between the (1 1 1) plane of fcc gold (0.235 nm) (JCPDS card No: 04-0784), and the fringe spacing of the NRs was 0.262 nm, corresponding closely with the spacing between the (0 0 2) plane of wurtzite ZnO (0.260 nm) (JCPDS card No: 36-1451). The selected-area electron diffraction (SAED) pattern of the Au NPs-decorated ZnO NRs is shown in Fig. S2. As revealed, the AuNPs-decorated ZnO NRs presented the diffraction spots, indicating single-crystalline wurtzite structure of ZnO NRs, and the diffuse rings of AuNPs.

The films changed their color from the opalescent to the brown after immersing in the dopamine solution (see Experimental Section, ESI), indicating the deposition of PDA films (Fig. S3). Moreover, after PDA coating, the sharp edges of the characteristic hexagonal morphology of ZnO NRs seemed almost indistinguishable (Fig. S4), and the fringe spacing of the NRs could not be clearly seen due to the presence of PDA films (Fig. 1c). The formed PDA thin layer on the AuNPs-decorated ZnO NRs had a mean thickness of ca. 6.5 nm, as shown in Fig. 1c. EDS analysis presented Zn, O, Au, and C peaks, attributing to ZnO, AuNPs, and PDA, respectively, as shown in Fig. S5. In addition, TEM analysis of a vertical nanorod, as shown in Fig. S6, revealed that the NRs remained the hexagonal morphology, indicating that the AP-assisted PDA deposition process had no discernible damage to ZnO NRs template.[1d]

After carbonization at 500 °C in N_2 and etching in dilute acid, the large-area and arrayed AuNP-embedded pBIDI-CNTs-modified films were obtained (Fig. 2a). The obtained pBIDI-CNTs were hollow and not open ended, as revealed from the inset of Fig. 2a. They also replicated the hexagonal morphology of ZnO NRs (Fig. 2b). The embedded AuNPs could be seen from Fig. 2b and Fig. S7. These observations indicate that the AuNPs sandwiched in the ZnO/AuNPs/PDA composites did not interfere with the template-directed carbonization of PDA to produce the arrayed AuNP-embedded pBIDI-CNTs.† Fig. 2c shows the side-view TEM image of the AuNPs-embedded pBIDI-CNTs. It can be seen that the carbon shell encapsulating the AuNPs had a thickness of ca. 5 nm, smaller than that of the PDA films, due to the shrinkage of PDA upon removal of the heteroatoms during the carbonization.[10] Several groups characterized recently the carbonized PDA films, presenting the typical BET surface areas ranged from ca. 500 to 800 m^2 g^{-1} with the pore size distribution centered at a value ranged from ca. 2 to 4 nm.[2a, 2b, 11] Therefore, the thin carbon shell formed here is considered to be favorable to mass transfer.[1a,1d] Zinc peak was not detected in EDS spectrum (Fig. S9) and XPS spectrum (Fig. S10). The pattern of the diffraction spots representing ZnO crystal also disappeared in the SAED pattern (Inset of Fig. 2c), indicating that hydrochloric acid was allowed to diffuse inside the tubes to dissolve ZnO, resulting in the formation of the hollow tubes.

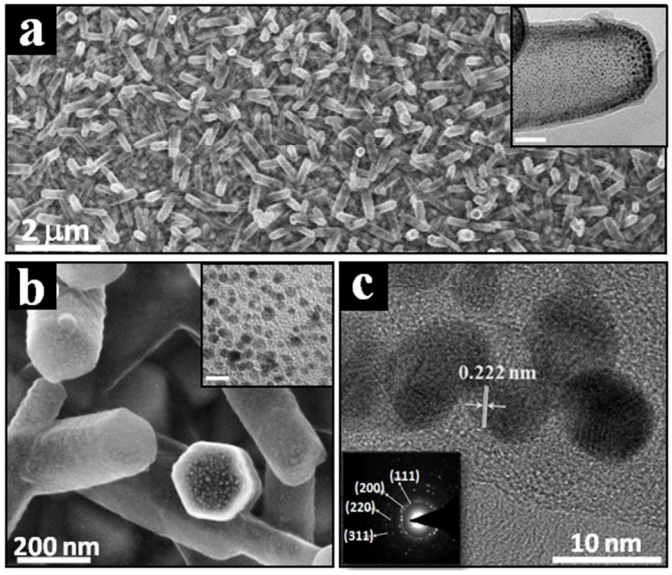

Fig. 2 Characterizations of the arrayed AuNPs-embedded pBIDI-CNTs: (a and b) SEM images with different magnification; Inset of a and b: high magnification TEM image (scale bar: 50 and 10 nm, respectively); (c) High magnification TEM image; Inset: SAED pattern of fcc gold.

Interestingly, even after undergoing a heat treatment, as shown in inset of Fig. 2b, the embedded AuNPs were still relatively uniformly distributed and had a high surface density to a level of ~ 9×10^{15} NPs · m^{-2}. More interestingly, as revealed in Fig. S11, the average size of the AuNPs was slightly increased to ~ 8.44 nm with σ of 2.99 nm (measured over 350 particles), indicating that the embedded high-density AuNPs did not aggregate severely. It is in sharp contrast to the cases of the unprotected AuNPs, which aggregate severely if the temperature is increased to above 300 °C.[12] For instance, Alexeyeva et al reported that the average size of the AuNPs synthesized by magnetron sputtering on the multi-walled CNTs was increased from ca. 11 nm to ca. 100 nm after thermal annealing at 400 °C.[13] Fullam et al reported that surfactant-capped gold NPs adsorbed on the CNTs also increased their average sizes from ca. 6 nm to more than 30 nm after heating at 300 °C just for 2 min.[10] Moreover, in our experiment, the embedded AuNPs were very crowded (~ 9×10^{15} NPs · m^{-2}), posing a great challenge to protection of them against sintering. Therefore, it is believed that the PDA-derived unique microstructures surrounding these high-density ultrafine AuNPs exert an important stabilizing effect. On the one hand, the high density AuNPs were sandwiched in the two-dimensionally confined space formed by the ZnO phase and the carbonized PDA phase; on the other hand, as aforementioned, the obtained hollow pBIDI-CNTs could replicate perfectly the hexagonal morphology of ZnO NRs template, suggesting that PDA has the excellent ability of imprinting templates. Indeed, it has been known that polydopamine can function as a surface imprinted polymer to imprint many materials, e.g., organic small molecules[14] and proteins[15]. Therefore, it is reasonable that the inner surface of the pBIDI-CNTs could possess the semispherical-like morphologies originated from the embedded AuNPs serving as the microtemplates during the PDA carbonization process (Fig. S12), and thus can grip the embedded AuNPs. Therefore, severe aggregation or sintering of the crowded NPs inside the tubes could be avoided.

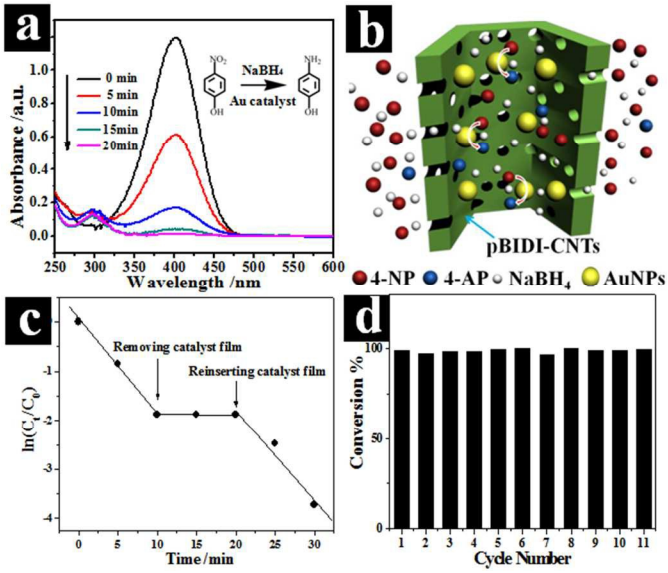

Fig. 3 (a) Time-dependent UV-vis absorption spectra of the 4-NP reduced by $NaBH_4$ catalyzed by the catalytic films. Inset: reaction scheme; (b) Schematic illustration of the NP-catalyzed reduction reaction; (c) Plot of $\ln(C_t/C_0)$ as a function of time, in an experiment in which the same catalyst film was removed and reinserted; (d) The conversions of 4-NP in 11 successive cycles with the catalytic films.

Catalytic activity of the obtained catalytic films was evaluated with 4-nitrophenol (4-NP) reduction by $NaBH_4$ to 4-aminophenol (4-AP) as a model. The reaction did not proceed without the catalyst.[1a] Upon immersing the catalytic films into the reaction mixture, the absorption at 400 nm quickly decreased, and absorption at 295 nm, ascribed to 4-AP,[16] increased accordingly (Fig. 3a). Meanwhile, the color of the solution changed from originally bright yellow to colorless after 20 min (Fig. S13). These observations indicate the efficiently catalytic activity of the AuNPs confined in the tubular nanoreactors, as schematically illustrated in Fig. 3b. The conversion process can be directly read off these absorption curves as the ratio of the concentration C_t of the 4-NP at time t to its value C_0 at $t = 0$ is directly given by the ratio of the respective absorbances A_t/A_0. In the case of an excess of $NaBH_4$, a pseudo-first-order rate kinetics with regard to the 4-NP concentration could be used to evaluate the catalytic rate of the catalytic films. As revealed from Fig. S14, a linear dependence of $\ln(C_t/C_0)$ vs reaction time was obtained. The apparent kinetic rate constant k_{app} was proportional to the total surface S of the embedded multiple AuNPs: $dC_t/dt = kC_t = k_1SC_t$, where k_1 was the rate constant normalized to S, the surface area of Au NPs normalized to the unit volume of the system. The k_{app} of this reaction could be directly calculated from the slope of this straight line to be 3.9×10^{-3} s^{-1}, which was comparable to previous AuNPs-based CNT membranes[17a] and AuNPs-based yolk-shell structured carbon spheres.[17b,17c] Switching the reaction off or on by the catalytic films was demonstrated in an experiment in which the catalyst film was removed and reinserted after a brief interval. As shown in Fig. 3c, the reaction was switched off upon removing the catalyst film from the reaction solution and did not proceed; the reaction was switched on upon reinserting the catalyst film in the reaction solution and proceeded with the unchangeable apparent kinetic rate. Catalytic performance stability or reusability was examined by recycling uses of the same catalytic film. Between each cycle, the catalyst film was directly withdrawn from the reaction solution and rinsed with deionized water. As revealed from Fig. 3d, almost identical catalytic activities with conversion near 100% within 20 min of reaction time were measured in 11 successive cycles, indicating the excellent recyclability of the catalytic films.

In conclusion, we have demonstrated for the first time fabrication of catalytic films comprising the catalyst-NP-embedded pBIDI-CNTs arrays with AuNPs as a model. The obtained catalytic films exhibited good catalytic activity and offered the feasibility and ease of multiple reuse. Because of the outstanding adhesion property of PDA and its template-directed carbonization ability, it is expected to apply this approach to introduce other NPs, regardless of their sizes and chemical compositions, inside the arrayed pBIDI-CNTs to produce catalytic films for NP-catalyzed applications.

The support from the NSF of China (No. 21175010 and 21275017), the Project-sponsored by SRF for ROCS, SEM, and the Program of Introducing Talents of Discipline to Universities (B14003), is highly appreciated.

Notes and references

[a] Research Center for Bioengineering and Sensing Technology, University of Science and Technology Beijing, Beijing 100083, China.
* E-mail addresses: sulei@ustb.edu.cn; zhangxueji@ustb.edu.cn.

† The presence of AuNPs may interfere with the carbonization of PDA. In a control experiment, PDA films were deposited on the ZnO NRs, followed by sputter deposition of AuNPs. Treating the resultant ZnO/PDA/AuNPs composites with the same carbonization and ZnO removal procedure, however, produced the collapsed tubes, as shown in Fig. S8. Relative investigation is under way in our lab.
Electronic Supplementary Information (ESI) available. See DOI: 10.1039/c000000x/

1 a) R. Liu, S. M. Mahurin, C. Li, R. R. Unocic, J. C. Idrobo, H. J. Gao, S. J. Pennycook, S. Dai, *Angew. Chem. Int. Ed.* 2011, **50**, 6799-6802; b) J.H. Kong, W.A. Yee, L.P. Yang, Y.F. Wei, S.L. Phua, H.G. Ong, J.M. Ang, X. Li, X.H. Lu, *Chem. Commun.* 2012, **48**, 10316-10318; c) K.L. Ai, Y.L. Liu, C.P. Ruan, L.H. Lu, G.Q. Lu, *Adv. Mater.* 2013, **25**, 998-1003; d) W. Gong, W.S. Chen, J.P. He, Y. Tong, C. Liu, L. Su, B.W. Gao, H.K. Yang, Y. Zhang, X.J. Zhang, *Carbon* 2015, **83**, 275-281; e) Y.R. Liang, H. Liu, Z.H. Li, R.W. Fu, D.C. Wu, *J. Mater. Chem. A* 2013, **1**, 15207-15211.

2 a) C. H. Xiao, X. C. Chu, Y. Yang, X. Li, X. H. Zhang, J. H. Chen, *Biosens. Bioelectron.* 2011, **26**, 2934-2939; b) G. Cheng, M. D. Zhou, S. Y. Zheng, *ACS Appl. Mater. Interfaces* 2014, **6**, 12719-12728; c) Y. Liu, K. Ai, L. Lu, *Chem. Rev.* 2014, **114**, 5057-5115; d) F. Bernsmann, J.C. Voegel, V. Ball, *Electrochim. Acta* 2011, **56**, 3914-3919; e)B.W. Gao, L. Su, Y. Tong, M. Guan, X.J. Zhang, *J. Phys. Chem. B* 2014, **118**, 12781-12787.

3 a) N. Liu, H. Wu, M. T. McDowell, Y. Yao, C. M. Wang, Y. Cui, *Nano Lett.* 2012, **12**, 3315-3321; b) D. G. Lee, S. M. Kim, H. Jeong, J. Kim, I. S. Lee, *ACS Nano* 2014, **8**, 4510-4521.

4 a) E. Hariprasad, T. P. Radhakrishnan, *Chem.-Eur. J.* 2010, **16**, 14378-14384; b) G. V. Ramesh, S. Porel, T. P. Radhakrishnan, *Chem. Soc. Rev.* 2009, ***38***, 2646-2656; c) L. Ouyang, D.M. Dotzauer, S.R. Hogg, J. Macanás, J.-F. Lahitte, M.L. Bruening, *Catal. Today* 2010, **156**, 100-106; d) X. Zhang, Z.H. Su, *Adv. Mater.* 2012, **24**, 4574-4577.

5 a) M. Pumera, *Chem.-Eur. J.* 2009, **15**, 4970-4978; b) G.G. Wildgoose, C. E. Banks, R.G. Compton, *Small* 2006, **2**, 182-193.

6 B. Sebez, L. Su, B. Ogorevc, Y. Tong, X. Zhang, *Electrochem. Commun.* 2012, **25**, 94-97.

7 a) K. Machado, J. Mishra, S. Suzuki, G.S. Mishra, *Dalton Trans.* 2014, **43**, 17475-17482; b) K. Xi, B.G. Chen, H.L. Li, R.S. Xie, C.L. Gao, C. Zhang, R. V. Kumar, J. Robertson, *Nano Energy* 2015, **12**, 538-546; c) C. Y. Chen, J.K. Chang, W.T. Tsai, C.H. Hung, *J. Mater. Chem.* 2011, **21**, 19063-19068.

8 a) X.L. Pan, X.H. Bao, *Acc. Chem. Res.* 2011, **44**, 553-562; b) F. Zhang, F. Jiao, X.L. Pan, K. Gao, J.P. Xiao, S. Zhang, X.H. Bao, *ACS catal.*

2015, **5**, 1381-1385; c) Z.J. Chen, Z.H. Guan, M.R. Li, Q.H. Yang, C. Li, *Angew. Chem. Int. Ed.* 2011, **50**, 4913-4917.

9 a) E. Castillejos, P.-J. Debouttière, L. Roiban, A. Solhy, V. Martinez, Y. Kihn, O. Ersen, K. Philippot, B. Chaudret, P. Serp, *Angew. Chem. Int. Ed.* 2009, **48**, 2529-2533; b) A. La Torre, M. W. Fay, G. A. Rance, M. D. Gimenez-Lopez, W. A. Solomonsz, P. D. Brown, A. N. Khlobystov, *Small* 2012, **8**, 1222-1228.

10 Y. F. Wei, J. H. Kong, L. P. Yang, L. Ke, H. R. Tan, H. Liu, Y. Z. Huang, X. W. Sun, X. H. Lu, H. J. Du, *J. Mater. Chem. A* 2013, **1**, 5045-5052.

11 a) H. Jiang, C. Z. Li, T. Sun, J. Ma, *Nanoscale* 2012, **4**, 807-812; b) L. J. Yan, X. J. Bo, Y. F. Zhang, L. P. Guo, *Electrochim. Acta* 2014, **137**, 693-699.

12 S. Fullam, D. Cottell, H. Rensmo, D. Fitzmaurice, *Adv. Mater.* 2000, **12**, 1430-1432.

13 N. Alexeyeva, J. Kozlova, V. Sammelselg, P. Ritslaid, H. Mandar, K. Tammeveski, *Appl. Surf. Sci.* 2010, **256**, 3040-3046.

14 L. Qiao, N. Gan, F. T. Hu, D. Wang, H. Z. Lan, T. H. Li, H. F. Wang, *Microchim. Acta* 2014, **181**, 1341-1351.

15 W. H. Zhou, C. H. Lu, X. C. Guo, F. R. Chen, H. H. Yang, X. R. Wang, *J. Mater. Chem.* 2010, **20**, 880-883.

16 J. J. Zhou, B. Duan, Z. Fang, J. B. Song, C. X. Wang, P. B. Messersmith, H. W. Duan, *Adv. Mater.* 2014, **26**, 701-705.

17 a) H.T Wang, Z.X. Dong, C.Z. Na, *ACS Sustainable Chem. Eng.* 2013, **1**, 746-752; b) K. Dong, Z. Liu, J.S. Ren, *CrystEngComm* 2013, **15**, 6329-6334; c) R. Liu, F.L. Qu, Y.L. Guo, N. Yao, R.D. Priestley, *Chem. Commun.* 2014, **50**, 478-480.

